# Valence fluctuation driven superconductivity in orthorhombic lead telluride

Liu-Cheng Chen,[1,2] Hao Yu,[1,2] Xin-Yu Wang,[3] Qian Zhang,[3] Viktor V. Struzhkin,[2] and Xiao-Jia Chen[1,2,*]

[1]*School of Science, Harbin Institute of Technology, Shenzhen 518055, China*

[2]*Center for High Pressure Science and Technology Advanced Research, Shanghai 201203, China*

[3]*School of Materials Science and Engineering, Harbin Institute of Technology, Shenzhen 518055, China*

(Received 2 December 2021; revised 11 April 2022; accepted 22 April 2022; published 2 May 2022)

Chemical doping or elemental substitution and applying pressure are considered to be two effective tools to create superconductivity from a parent compound. The latter is more powerful than the former for contracting the lattice but does not bring about impurities, defects, or disorders compared with the former, thus serving as a good platform to examine or test any theoretical models for the born superconductivity. Among the various theories proposed for superconductivity, the electron-phonon interactions (or phonon mediated), spin fluctuations (or spin mediated), and valence fluctuations (or valence mediated) are the three major mechanisms. The first two have received extensive support from many elements and compounds over the last century, and only a few examples are believed to be a result of valence fluctuations. Lead telluride (PbTe), a Group IV-VI compound, is being examined as a promising candidate whose superconductivity is mediated by the valence fluctuations. The superconductivity has been reported in doped PbTe with the rocksalt NaCl structure at ambient pressure or parent PbTe with the body-centered cubic CsCl structure at high pressure. The pressure-driven intermediate orthorhombic phase in between has been known as a semiconductor with a large band gap and no expectation for the appearance of superconductivity. By doping I in the Te site to adding more carriers and partially substituting Pb by In with the expected valence change, however, we show that the co-doped PbTe exhibits superconductivity upon compression in the orthorhombic phase besides the expected one with the CsCl structure. Through the systematic studies of the structural, vibrational, electrical, and superconducting properties, we suggest that the observed superconductivity in the orthorhombic phase is mediated by the valence fluctuations associated with mixed valency on the In sites. This work thus not only offers an example for valence-mediated superconductivity but also fills the gap for the superconducting phase of PbTe in between the NaCl and CsCl structure.

DOI: 10.1103/PhysRevB.105.174503

## I. INTRODUCTION

As a star material among the Group IV-VI compounds, PbTe has been attracting tremendous interest for a long time due to its fascinating physical properties and technological applications [1]. It keeps the starting rocksalt NaCl structure upon doping at ambient pressure but exhibits extraordinary properties as highly efficient thermoelectric materials [2–4], topological crystalline insulators [5–8], and especially the superconductors [9]. Upon heavy doping or adding more carriers through the substitution of Tl in Pb sites, superconductivity with the transition temperature $T_c$ as high as 1.5 K was found [9]. Interestingly, the charge Kondo fluctuations close to $T_c$ were also reported by the temperature and field dependencies of the resistivity upturn [9,10], the anomaly in thermoelectric power [11], and the theoretical calculations [12,13]. A static mixed-valence model ($Tl^{1+}$, $Tl^{3+}$) [14,15] was proposed to explain these interesting features through a negative effective $-U$, where $U_n = (E_{n+1} - E_n) - (E_n - E_{n-1}) < 0$ with $n$ being the valence state [16,17]. This picture was later supported by the observed valence change from the photoemission spectroscopy measurements [18,19]. Meanwhile, the electron-phonon interaction seemingly cannot be ruled out as responsible for the observed superconductivity [10].

Similar to the effects brought through the chemical doping or elemental substitution, the superconductivity can also be achieved in these Group IV-VI compounds solely by the application of pressure [20,21]. One may wonder whether the valence fluctuations in PbTe-based materials also work for the superconductivity in other phases at high pressures. Upon compression, PbTe experiences the similar evolution path with pressure as other Group IV-VI compounds: first from the rocksalt NaCl structure ($B1$ with space group $Fm\bar{3}m$) to a lower symmetrical phase (*Pnma*) and then going from the *Pnma* phase to body-centered cubic (*bcc*) CsCl structure ($B2$ with space group $Pm\bar{3}m$) [20,22–24]. These structural features correspond to the semiconducting behavior with narrow band gaps for the first two phases and the metallic state for the last phase [25,26]. As pressure is increased, a huge reduction of the resistivity is observed in the initial $B1$ phase of PbTe followed by the steep increase for the intermediate *Pnma* phase before suddenly dropping in the $B2$ phase [21,27,28], in good agreement with the structural characters and phase behavior[22–24]. So far, pressure-induced superconductivity was reported only in the last $B2$ phase of PbTe [21]. The large resistivity in the intermediate *Pnma* phase of this compound [21,27,28] is not in favor of superconductivity. The $B2$ phase

*xjchen2@gmail.com

 

seemingly is only left for the examination of the role of the valence fluctuations played for the superconductivity in PbTe-based compounds. In this work, In-I co-doped PbTe is chosen for the study of the superconductivity at high pressures along with the examination of the associated mechanism(s). Here, a Group III A element In is selected with the expectation of sharing the same feature as Tl [9]. The element I is added to substitute Te for the increase of the carrier concentration in the studied system [4]. The compound with the composition of $In_{0.0035}Pb_{0.9965}Te_{0.996}I_{0.004}$ is chosen due to its excellent thermoelectric figure of merit at room temperature [4] and thus is expected to exhibit the desired superconducting properties based on the recent studies [20,29–32].

## II. EXPERIMENTAL METHODS

The In-I–codoped PbTe used in this study was synthesized with the nominal compositions $In_{0.0035}Pb_{0.9965}Te_{0.996}I_{0.004}$ by melting, hand milling, and hot pressing. The detailed synthesizing method can be obtained elsewhere [4]. At high pressures, the synchrotron x-ray diffraction (XRD) patterns were collected at the PETRA III beamline P02.2 at Deutsches Elektronen-Synchrotron (DESY), Hamburg. The wavelength was chosen as 0.2910 Å. Here, the high pressures of this study were generated by a symmetrical diamond-anvil cell (DAC) with the 300 $\mu$m culets. The pressure-transmitting medium in the sample chamber was neon. The obtained two-dimensional XRD patterns were integrated into the one-dimensional function with the help of the DIOPTAS software [33]. The data were further analyzed by using the software of Jana based on the Rietveld method [34].

The temperature-dependent resistivity at ambient pressure was measured by a thermal transport option setup in a Physical Property Measurement System (PPMS) from Quantum Design. The measurements of high-pressure electrical resistivity ($\rho_{xx}$) and Hall resistivity ($\rho_{xy}$) were also performed by using the PPMS. The high pressures for the electrical measurements were realized by a nonmagnetic DAC with anvils of 300 $\mu$m culets [35]. The diameter of about 150 $\mu$m of the sample chamber was made from T301 steel. The steel gasket was electrically insulated by using the mixture of the cubic boron nitride and epoxy. The size of the sample was about $80 \times 80 \times 20$ $\mu m^3$. A small ruby ball was loaded into the sample chamber for calibrating the pressure. To maintain the hydrostatic pressure environment, daphne oil 7373 was loaded in the hole as a pressure-transmitting medium. The van der Pauw method was used to accurately obtain the resistivity at high pressures [36]. The zero-resistivity state for the character of superconductivity was previously obtained for many compounds at high pressures by using this technique [20,30–32].

## III. THEORETICAL CALCULATIONS

To unveil the origin of the superconductivity observed in this material under pressure, we carried out density-functional theory calculations on In- and/or I-doped PbTe by using the Vienna *Ab initio* Simulation Package (VASP) [37]. For accurately modeling the co-doped PbTe, we enlarged the primitive cell to a $2 \times 2 \times 2$ supercells. We first optimized the geometry and volume of the supercell with 64 atoms (32 Pb and 32 Te), and then the In and I were introduced to replace Pb and Te, respectively. All the atomic positions were fully relaxed to their ground-state configurations, then we calculated the band structures and the corresponding density of states at high pressures. The generalized gradient approximation (GGA) of Perdew, Burke, and Ernzerhof (PBE) was used for the exchange-correlation functional [38]. The cutoff energy of the plane-wave basis was set to 520 eV. A centered $4 \times 3 \times 2$ Monkhorst-Pack grid was used for the geometry relaxation and self-consistent field (SCF) calculations.

## IV. RESULTS AND DISCUSSIONS

To determine the high-pressure structural behavior, we performed XRD measurements on $In_{0.0035}Pb_{0.9965}Te_{0.996}I_{0.004}$ at high pressures. As can be seen, all the Bragg peaks shift to larger angles, showing the shrinkage of the lattice [Fig. 1(a)]. Depending on the changes in the diffraction patterns, two obvious phase transitions can be observed around 7 and 20 GPa, respectively. The initial phase of this sample is found to be stable up to 6.2 GPa. Upon compression, the XRD patterns reveal significantly different features between 7.3 and 20.2 GPa, suggesting the occurrence of a new phase. Above 22 GPa, another phase transition takes place, as indicated by the unexpected characters of the XRD patterns. When the pressure is released to 0.5 GPa, the XRD patterns recover to the profile at ambient pressure, indicating the reversible process. The refined results at the selected pressure of 1.3, 10.2, and 27.3 GPa by using the Rietveld method are shown in Fig. 1(b). Three phases with the space group of $B1$, *Pnma*, and $B2$ are demonstrated by the reasonable refinements. The Rietveld refinements yield the factors of $R_p = 2.15\%$, $R_{wp} = 2.25\%$, and $\chi^2 = 1.54$ for the $B1$ phase, $R_p = 4.21\%$, $R_{wp} = 3.76\%$, and $\chi^2 = 1.31$ for the *Pnma* phase, and $R_p = 1.16\%$, $R_{wp} = 2.34\%$, and $\chi^2 = 1.14$ for the $B2$ phase.

The pressure-dependent lattice parameter and volumes are plotted in Fig. 2(b). Two coexistence regions (7.3–8.5 and 20.2–24.2 GPa) can be seen around the phase transitions. The volume evolution with pressure is fit by using the Murnaghan equation of states [39]:

$$P = \frac{3B_0}{2}\left[\left(\frac{V}{V_0}\right)^{7/3}\right]\left\{1 + \frac{3}{4}(B_0' - 4)\left[\left(\frac{V}{V_0}\right)^{2/3} - 1\right]\right\}, \quad (1)$$

where $V_0$, $B_0$, $B_0'$ are the unit-cell volume, bulk modulus, and first-order derivative of the bulk modulus at ambient pressure, respectively. The fitting yields $V_0 = 67.121(2)$ Å$^3$, $B_0 = 38.720(4)$ GPa, and $B_0' = 5.176(2)$ for the $B1$ phase, $V_0 = 65.446(3)$ Å$^3$, $B_0 = 40.235(5)$ GPa, and $B_0' = 3.594(6)$ for the *Pnma* phase, and $V_0 = 60.374(5)$ Å$^3$, $B_0 = 47.800(3)$ GPa, and $B_0' = 4.333(2)$ for the $B2$ phase. Here, the number of formula units per unit cell $Z$ was induced to denote the systematic change of the volume of the different phases upon compression. The $Z$ value is four for both the $B1$ and *Pnma* phase, and one for the $B2$ phase. The volume collapses from the $B1$ to *Pnma* phase and from the *Pnma* to $B2$ phase 3.5% and 3.7%, respectively, indicating that both structural transitions are first order.

Note that the lattice period of the *Pnma* structure of this sample has an approximately doubled relationship with the $B1$ phase [Fig. 2(b)]. The *Pnma* structure of PbTe can be

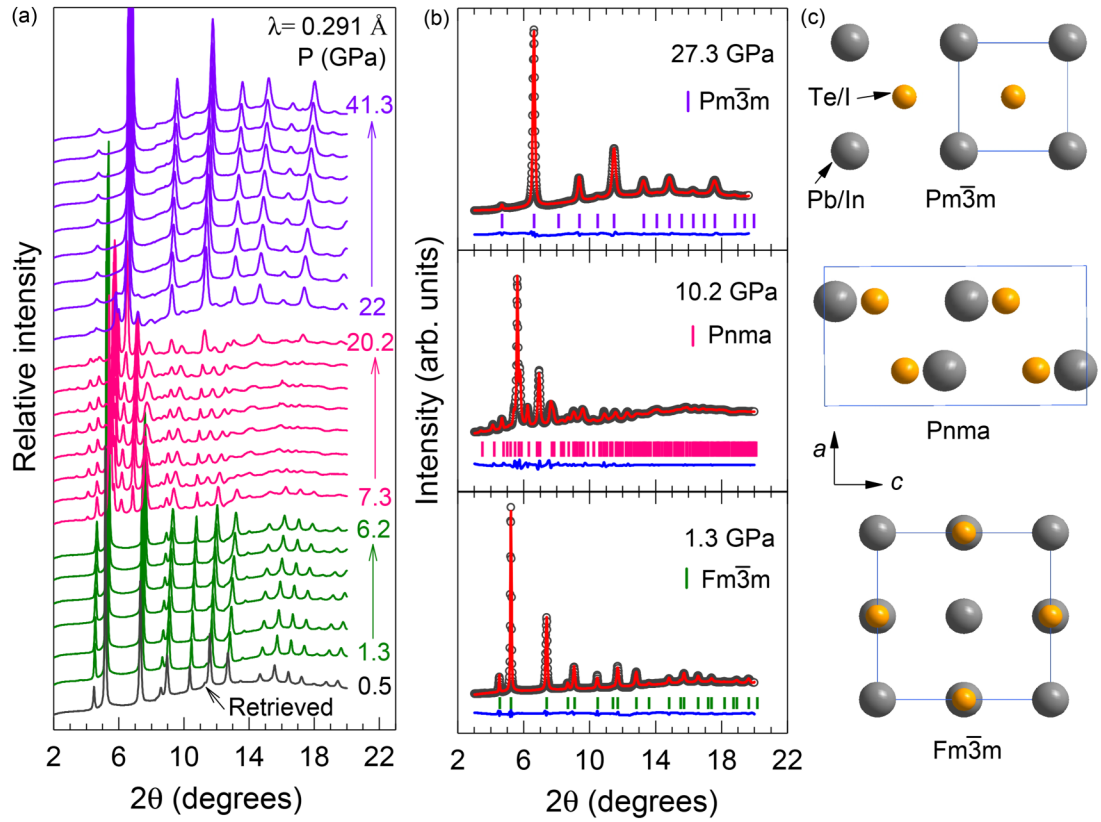


FIG. 1. The structures of $In_{0.0035}Pb_{0.9965}Te_{0.996}I_{0.004}$ at high pressure. (a) High-pressure synchrotron XRD patterns at pressures ranging from 1.3 to 41.3 GPa. The gray spectra represent the XRD patterns obtained at 0.5 GPa. (b) Representative Rietveld refinements of the XRD patterns at 1.3, 10.4, and 27.3 GPa, respectively. The open circles are the experimental data points. The red curves are the calculated results based on the different structures. The sticks in each panel are the Bragg-peak positions. The thin curves at the bottom of each panel are the deviations between experiments and calculations. (c) The structures of the *B*1, *Pnma*, and *B*2 phase. The gray circles are the Pb (In) atoms and yellow circles are the Te (I) atoms.

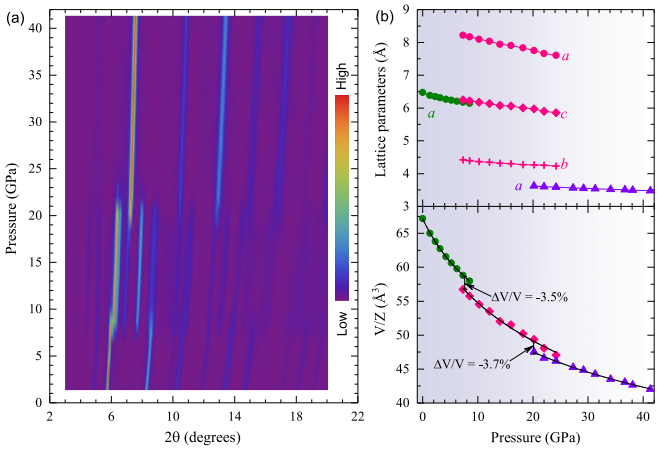


FIG. 2. Crystal structures of $In_{0.0035}Pb_{0.9965}Te_{0.996}I_{0.004}$ at high pressures. (a) Synchrotron XRD patterns of the sample at room temperature and various pressures up to 42 GPa. The red and blue colors represent the high and low diffraction intensity, respectively. (b) Pressure-dependent lattice parameter(s) and unit-cell volume in the *B*1, *Pnma*, and *B*2 phases. The thin curves represent the fitted results for the pressure dependence of volume. $\Delta V/V$ represents the volume collapse from the *B*1 to *Pnma* phase (7.2%) and from the *Pnma* to *B*2 phase (8.1%), respectively.

created by an orthorhombic distortion of the *B*1 phase [24]. The doubled period of the *Pnma* lattice is thus driven by a Peierls distortion of the initial *B*1 phase [23]. Such a relationship of the *Pnma* and *B*1 phase was also observed in Cr-doped PbSe [20,40]. The reported superconductivity in the *B*2 phase of this sister was proposed to result from the melting of the lattice distortion. Within the same structure picture, the superconductivity is also highly expected in the *B*2 phase for In-I co-doped PbTe due to the similar structural evolution process. In addition, due to the participation of the valence skipping element In, this material serves as a good candidate for exploring valence fluctuation driven superconductivity.

In the *B*1 phase [Fig. 3(a)], the temperature-dependent resistivity $\rho$ at ambient pressure shows a metallic character, which is consistent with the behavior reported earlier [4]. At low pressure, $\rho$ is continuously suppressed below 3.6 GPa. Meanwhile, a broad hump around 150 K becomes obvious with increasing pressure. At 4.8 GPa, $\rho$ is further suppressed but behaves in an insulating manner. The abnormal phenomenon around 4.8 GPa does not originate from a structural transition (Figs. 1 and 2). This is associated with the pressure-driven topological phase transition, as reported for the PbSe compound [20,40]. Applying pressure suppresses the insulating behavior and an insulator-metal transition takes place around 180 K at pressure of 6.1 GPa. The increased

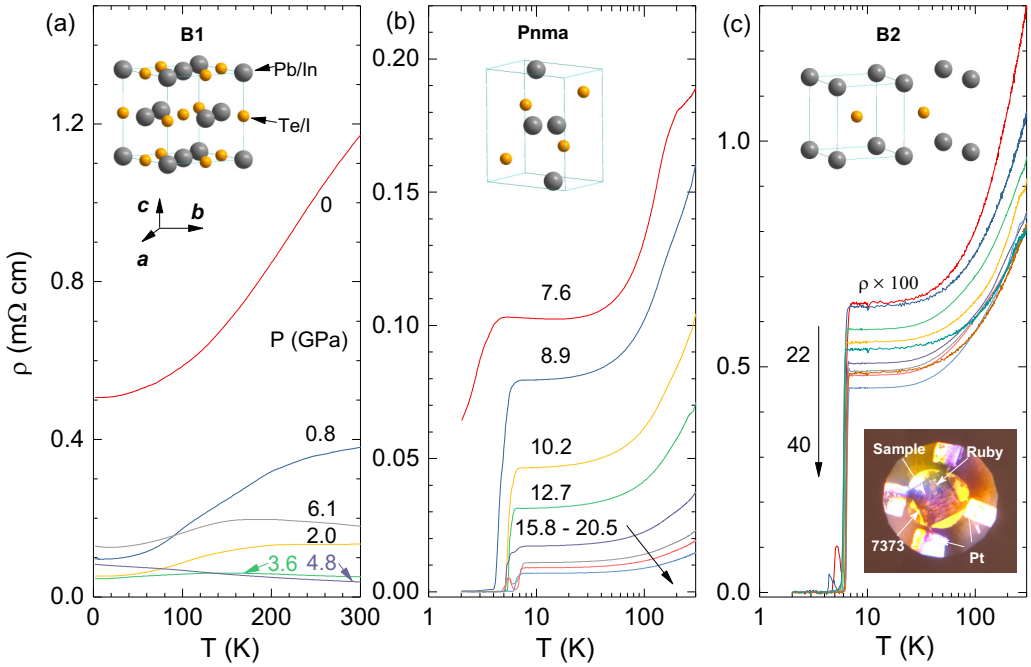


FIG. 3. Temperature dependence of the resistivity for (In,I)-doped PbTe at various pressures up to 40 GPa. (a) Temperature-dependent resistivity at pressures from 0 to 6.1 GPa in the $B1$ phase. (b) Temperature-resistivity curves for pressures from 7.6 to 20.5 GPa in the *Pnma* phase. The drop of the resistivity and zero-resistivity behavior can be observed at low temperatures. (c) Temperature-dependent resistivity at pressures from 22 to 40 GPa in the $B2$ phase. The upper insets show the crystal structures of the (a) $B1$, (b) *Pnma*, and (c) $B2$ phase, respectively. The low inset of panel (c) shows the actual setup for the electrical transport measurements between a pair of diamond anvils under pressure. Four thin platinum probes are attached to the sample, the Daphne oil 7373 is loaded for the pressure-transmitting medium, and the loaded ruby ball is used for pressure calibration.

$\rho$ and the insulator-metal transition indicate an incomplete phase transition from the $B1$ to *Pnma* phase. In the *Pnma* phase, the insulator-metal transition gradually disappears, and the metallic character is maintained above 7.6 GPa [Fig. 3(b)]. At the same time, a sudden drop of the $\rho$ can be clearly seen at this pressure with a transition temperature ≈5.3 K. Accompanied by the gradual reduction of $\rho$, the resistivity drop becomes more evident with increasing pressure. At 8.9 GPa, zero resistivity at low-temperatures is observed, suggesting the occurrence of superconductivity in the studied system. After 15.8 GPa, another superconducting transition takes place with a higher superconducting transition temperature ($T_{c2}$). This superconducting transition is related to the second phase transition from the *Pnma* to $B2$ structure. The $T_{c2}$ becomes more prominent upon heavy compression. Meanwhile, the first superconducting transition temperature ($T_{c1}$) is gradually suppressed until 25 GPa and disappears at higher pressures. The resistivity at the normal state in the $B2$ phase does not change too much with increasing pressure [Fig. 3(c)]. The two superconducting phases have a large coexisting range from 15.8 to 25 GPa. The resistivity measurements also yield the phase boundary for the coexistence of the *Pnma* and $B2$ structure. The two superconducting transitions are confirmed by the magnetic field dependence of electrical resistivity [Figs. 4(a) and 4(b)]. For the $T_{c2}$ behavior in the $B2$ phase, the upper critical field at the absolute zero temperature [$H_{c2}(0)$] is given with the Werthamer-Helfand-Hohenberg equation [41]: $H_{c2}(0) = 0.693[-(dH_{c2}/dT)]_{T_c}T_c$. The calculated $H_{c2}(0)$ is about 6 T at 30 GPa. This value is comparable with that of the superconducting $B2$ phase in the sister PbSe [40]. The maximum $T_{c2}$ for the $B2$ phase is about 7.5 K at around 18 GPa. This is in agreement with the $T_c \approx 8$ K at 17.5 GPa in the $B2$ phase of undoped PbTe [21]. The consistent $T_c$ values between $In_{0.0035}Pb_{0.9965}Te_{0.996}I_{0.004}$ and parent PbTe in the same $B2$ phase indicate that the superconductivity is an intrinsic effect of PbTe at high pressures rather than the contributions from either In or I or both. In consideration of the phenomena observed in PbSe [20], the superconductivity in the $B2$ phase for this material should be a result of the melting of the lattice distortion from the previous *Pnma* structure. However, the realization of superconductivity in the *Pnma* phase for this material is not expected at high pressures either from early experiments or theoretical predications [20,21]. Therefore, the observed superconductivity in the *Pnma* phase is brought by the doping element(s).

To explore the linkage between the $T_{c1}$ and the impurities in the *Pnma* phase, we carried out the first-principles calculations on this material at high pressures. The calculated band structures of PbTe at 7.5 GPa show a typical semiconductor character with an indirect band gap along the Y-Γ direction [Fig. 5(a)], indicating that the superconductivity in the *Pnma* phase is due to the contribution from the impurities. As shown in Figs. 5(b) and 5(c), the Fermi level ($E_F$) of I-doped PbTe shifts up to the conduction band. This demonstrates that the incorporation of I noticeably improves the carrier concentration. The excellent thermoelectric performance of this material clearly benefits from this improvement [4]. If the impurity I is replaced by In ($InPb_{31}Te_{32}$), a localized band with a flat-band

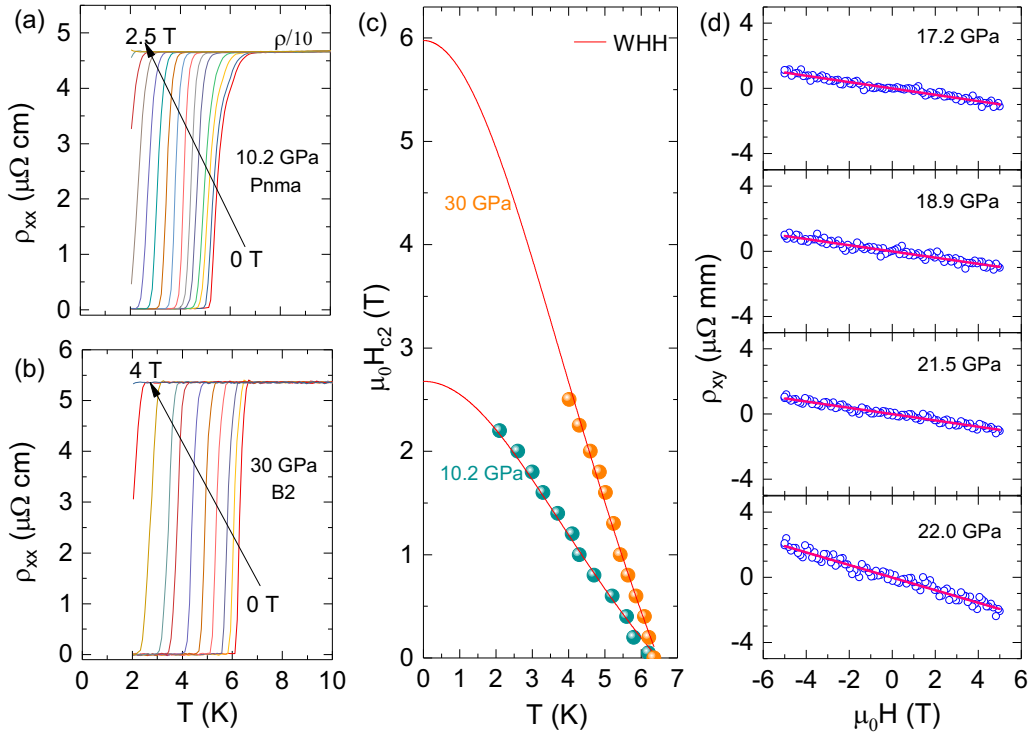


FIG. 4. Magnetic-field dependencies of the resistivity ($\rho_{xx}$) and Hall resistivity ($\rho_{xy}$) of (In, I)-doped PbTe at high pressures. (a), (b) Magnetic-field dependence of $\rho_{xx}(T)$ at pressure of 10.8 GPa in the *Pnma* phase and 25 GPa in the *B*2 phase, respectively. (c) The upper critical field $H_{c2}$ as a function of temperature at pressure of 10.8 and 25 GPa, respectively. $T_c$ was determined from the 90% resistivity transition. The red line represents the calculated $H_{c2}$ from the Werthamer-Helfand-Hohenberg (WHH) equation. (d) Magnetic-field dependence of $\rho_{xy}$ at temperature of 10 K for selected pressures. The blue circles represent the raw data points and the red lines are the linear fitting to the data. The almost parallel curves indicate the almost equivalent Hall coefficients ($R_H$), and thus the carrier concentration ($n_H$).

character appears on the top of the conduction band in the band-gap region [Fig. 5(c)]. Furthermore, two localized bands of states can be observed in the density of states (DOS) curve [Fig. 6(d)]. One locates below the valence-band minimum and the other above the valence-band maximum but lying in the band-gap region. Such localized bands of states, which were also called the deep defect states, have been observed in the DOS curves in the lead chalcogenides upon substitution by the valence-skipping element in their rocksalt structure [42,43].

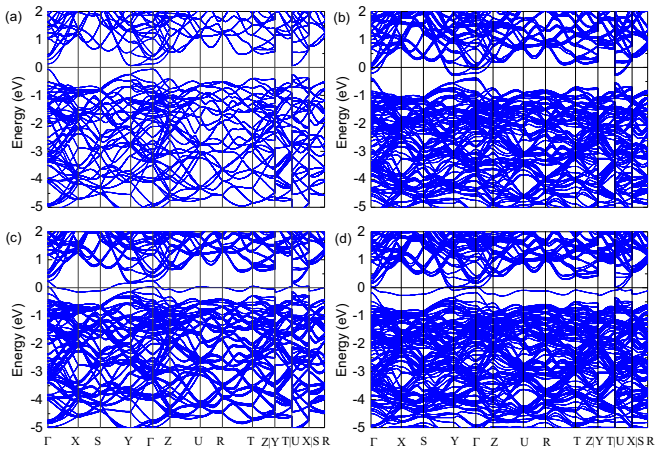


FIG. 5. The electronic band structures of (a) $Pb_{32}Te_{32}$, (b) $Pb_{32}Te_{31}I$, (c) $InPb_{31}Te_{32}$, and (d) $InPb_{31}Te_{31}I$ at 7.5 GPa in the *Pnma* phase.

The electronic band structures of In-I co-doped PbTe were calculated at pressure of 7.5 GPa [Fig. 5(d)]. The localized bands of In-I co-doped PbTe are still in the band-gap region except a narrow overlapping with the conduction band between the high-symmetry point Y and Γ. Meanwhile, the $E_F$ of the In-I co-doped PbTe moves up slightly and locates at the bottom of the conduction band. Compared with the calculated results of the In- and I-doped PbTe, the localized bands of states (around $E_F$) in the DOS curve of In-I co-doped PbTe are found to be associated with the dopant element In in PbTe [Fig. 6(e)]. In addition, the *p* character of Te changes dramatically in the presence of In [Fig. 6(f)]. This partial DOS of Te *p* has a similar shape with the localized band states. As seen from Figs. 6(e) and 6(f), the large DOS for In-I co-doped PbTe is mainly composed of the hybridization of the In-*s* and Te-*p* state, other than the contributions from the impurity I. This hybridized state is supported by the bonding state between the impurity In and the neighboring Te atoms [Fig. 6(b)]. Thus, these calculations indicate that the superconductivity in (In, I)-doped PbTe within the *Pnma* structure is mostly related to the valence-skipping character of In. In the following, we show how the valence fluctuations drive superconductivity in this phase.

The element In also shares the valence-skipping character that tending to skip the +2 valence, and in favor of +1

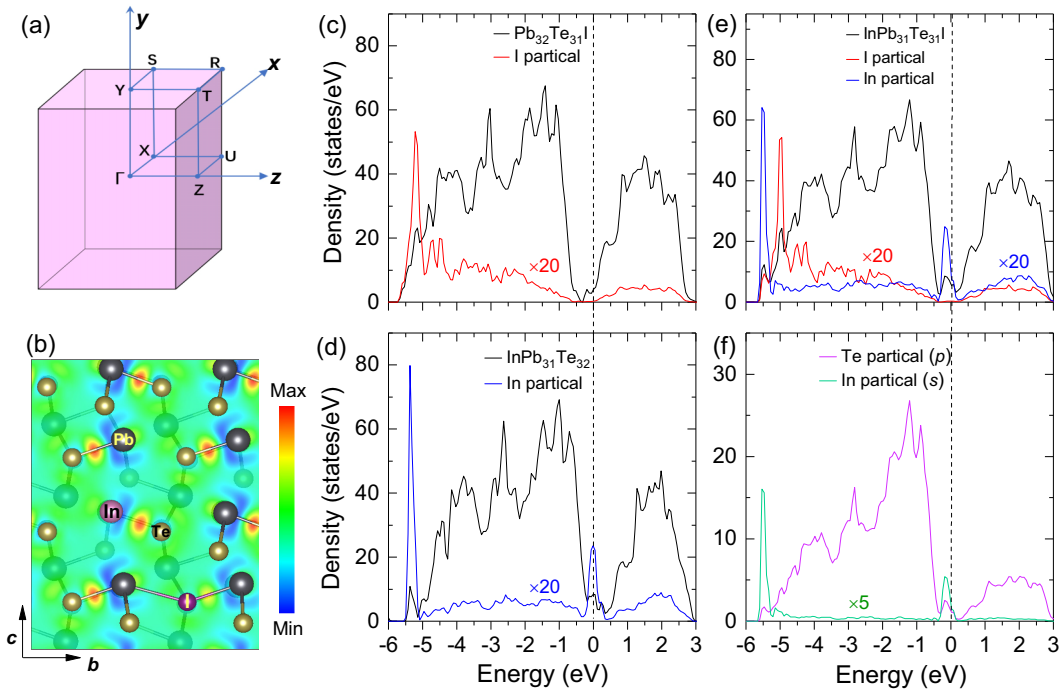


FIG. 6. Calculated electronic band structures of (In, I)-doped PbTe in the *Pnma* phase. (a) The Brillouin zone for the *Pnma* phase. The high-symmetry points for the band-structure calculations are marked in the Brillouin zone. (b) Deformation electronic density in $InPb_{31}Te_{31}I$. The values in the red and blue are positive and negative, respectively. An banding state can be clearly seen between In and its neighboring Te. (c) Total density of states (DOS) of $Pb_{32}Te_{31}I$ and the partial DOS associated with the I atom. (d) Total DOS of $InPb_{31}Te_{32}$ and the partial DOS associated with the In atom. (e) Total DOS of $InPb_{31}Te_{31}I$ and the partial DOS associated with the I and In atom. The partial DOS is multiplied by a factor of 20 for the clear demonstration. (f) In partial DOS associated with the *s* orbital and Te partial DOS associated with the *p* orbital character.

and +3, such as the case in InCl and $InCl_3$. Such a mixed valence state has been demonstrated in the rocksalt structure of the high-pressure synthesized $Pb_{1-x}In_xTe$ and $Ge_{1-x}In_xTe$ by using x-ray photoelectron spectroscopy and photoemission spectroscopy measurements, respectively [44,45]. Generally, the participation of valence skipping elements is more favor of the superconductivity with higher $T_c$, such as $Pb_{1-x}Tl_xTe$ ($x = 1.5\%$, $T_c = 1.5$ K) [9,10], $In_{1-x}Pb_xTe$ ($x = 0.6$, $T_c = 5.1$ K) [46], $Sn_{1-x}In_xTe$ ($x = 0.4$, $T_c = 4.4$ K) [47], etc. For the studied *Pnma* $In_{0.0035}Pb_{0.9965}Te_{0.996}I_{0.004}$, the maximum value of $T_{c1}$ is 6.3 K at pressure of 10.2 GPa. This high-pressure $T_{c1}$ is much higher than the $T_c$ values observed in the chemical substitution induced superconductivities for other semiconductors, such as PbTe, SnTe, InTe, and GeTe [21]. Thus, the anomalously high $T_{c1}$ value supports the existence of valence fluctuation pairing associated with the In dopant in the studied system. In addition, for the valence skipping elements participated superconductivity, the abnormally low upper critical fields are often observed. Typical examples are $Pb_{1-x}Tl_xTe$, $H_{c2}(0) \simeq 0.6$ T with $T_c \simeq 1.5$ K [9,10], $Pb_{1-x}In_xTe$, $H_{c2}(0) \simeq 3$ T with $T_c \simeq 5$ K [46], $Sn_{1-x}In_xTe$, $H_{c2}(0) \simeq 1.46$ T with $T_c \simeq 4.4$ K [47], etc. These low $H_{c2}(0)$ values cannot be explained well within the BCS framework because they are lower than the expectations from the weak-coupling Pauli limit [48]: $\mu_0 H_{Pauli} = 1.85 \times T_c$. Based on the Werthamer-Helfand-Hohenberg equation [41], we obtained the $H_{c2}(0)$ of only about 2.5 T at 10.2 GPa for the studied material in the *Pnma* phase [(Fig. 4(c)]. This value is much lower than the weak-coupling Pauli limit. Meanwhile, the $T_{c1}$ and $T_{c2}$ values of this sample at 10.2 and 30 GPa are almost the same, but the $H_{c2}(0)$ at 10.2 GPa is less than half of that at 30 GPa [(Fig. 4(c)]. The large difference of $H_{c2}(0)$ at these two pressures indicates the different origins of the superconductivity in these two high-pressure phases. In other words, the emergence of the superconductivity in the *Pnma* phase is not mainly controlled by the electron-phonon coupling.

Then, the $n_H$, which tightly connects with the DOS at the $E_F$, plays an important role in understanding the superconductivity for a material [49]. For example, a remarkable feature for confirming the mixed valence in $Pb_{1-x}Tl_xTe$ is the evolution of $n_H$ with TI concentration $x$. For $x < x_c$ ($x_c \approx 0.3\%$), the concentration of holes grows linearly with $x$. For $x > x_c$, $Pb_{1-x}Tl_xTe$ becomes superconducting with a maximum $T_c \approx 1.5$ K, and the concentration of holes appears to approach the saturation, suggesting that the additional impurities act in a self-compensating manner [9,13]. Generally, the $n_H$ can be obtained by using the equation $n_H = 1/eR_H$, where $e$ and $R_H$ are the unit of charge and Hall coefficient, respectively. The $R_H$ can be obtained by fitting the magnetic-field-dependent Hall resistivity under pressure. In Fig. 4(d), the Hall resistivity curves of this sample at the selected pressures are almost parallel. These parallel Hall resistivity curves illustrate the almost equal value of $R_H$, and

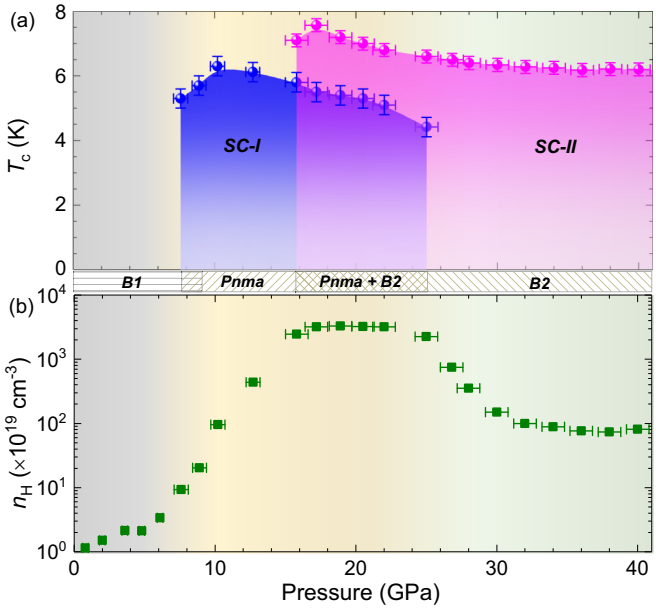


FIG. 7. Temperature-pressure phase diagram of (In, I)-doped PbTe. (a) The evolution of $T_c$ with pressure. (b) Pressure dependence of the carrier concentration $n_H$ measured at temperature of 10 K in the different phases indicated by the space groups in the region between the upper and lower panels.

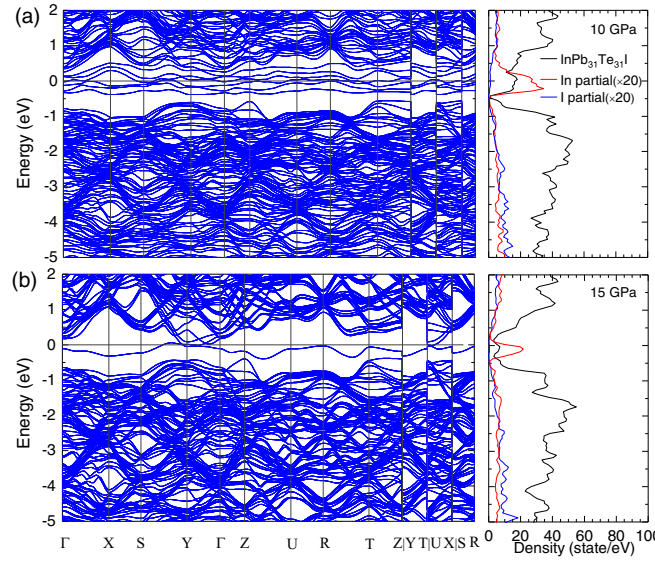


FIG. 8. The electronic band structures and density of states of $InPb_{31}Te_{31}I$ at the pressures of (a) 10 and (b) 15 GPa in the *Pnma* phase.

thus the equivalent $n_H$. The almost unchanged $n_H$ values at selected pressures provide reliable evidence for the existence of the mixed valence ($In^+$, $In^{3+}$) in the *Pnma* phase of this material.

Combined with the resistivity and x-ray diffraction measurements, we can map out the phase diagram of $In_{0.0035}Pb_{0.9965}Te_{0.996}I_{0.004}$ under pressure [Fig. 7(a)]. Within the studied pressure range, three phases can be clearly seen, which are the *B*1, *Pnma*, and *B*2 phase, respectively. In the initial phase, this material presents a complex temperature-dependent electrical transport properties for pressures below 7 GPa. These complex behavior can be attributed to the topological phase transition and the entrance of the topological crystalline insulator [25], as early reported in the compressed PbSe [40]. After that, two distinct superconducting phases with the *Pnma* and *B*2 structure can be observed. The first dome shapes the first superconducting phase (SC-I) with the pressure range from 7.5 to 25 GPa. The $T_{c1}$ of SC-I first emerges at 7.5 GPa with $T_{c1} \approx 5.3$ K and then increases to 6.3 K upon compression at 10.8 GPa. After passing the maximal $T_{c1}$, it is suppressed continuously until it cannot be detected above ≈25 GPa. Above 15.8 GPa, another superconducting phase (SC-II) emerges with a metallic normal state and persists up to the highest pressure (40.5 GPa) in this study. Overall, the $T_c$ in SC-II first exhibits a domelike shape with pressure and then decreases slightly upon heavy compression. Different from the coexistence region for the *Pnma* and *B*2 phase detected by XRD, the resistivity measurements reveal a large coexistence range for the SC-I and SC-II. This difference may come from the different transmitting media used in these experiments, as illustrated in the methods section.

The $n_H$ values at high pressures were obtained by fitting the Hall resistivity [Fig. 7(b)]. The sign of the calculated $n_H$ at 10 K is negative in the studied pressure region. This provides the dominant electron character for the two superconducting phases. This electron character is supported from the theoretical calculations (Figs. 5 and 6). Note that the $n_H$ value does not change too much with increasing pressure in the *B*1 phase. Here, the kink around 4 GPa is due to the topological phase transition as mentioned in the temperature-resistivity behavior [Fig. 3(a)]. When entering the *Pnma* phase, $n_H$ has an obvious increase upon compression until to 16 GPa, and then levels off with increasing pressure up to 25 GPa. The saturated $n_H$ together with the high $T_c$ and low $H_{c2}(0)$ indicates that the valence fluctuation associated with valence skipping states of In is the major driving force for superconductivity in the *Pnma* phase.

In addition, from Figs. 6 and 8, we can note that the DOS at the bottom of the conduction band is largely enhanced at 10 GPa, and the breadth of the DOS becomes wider compared with that at 7.5 GPa. The large DOS near the band gap is consistent with the increased $n_H$ and thus increased $T_{c1}$ (Fig. 7). At 15 GPa, the $E_F$ shifts back to the bottom of the conduction band, which shares the characters of the band structures at 7.5 GPa. Meanwhile, the DOS at this pressure becomes weak, corresponding well to the decreasing $T_{c1}$ behavior with increasing pressure in the *Pnma* phase (Fig. 7). Thus, the evolution of the band structure with pressure provides a clue to the electron-phonon interaction as the joint player with the valence fluctuations to the superconductivity in the *Pnma* phase. The electron-phonon interaction was also emphasized in the superconductivity of TI-doped PbTe system. Depending on the heat capacity and electrical transport measurements, TI-doped PbTe was identified to be a type II, weak-coupled BCS superconductor [10]. The observed localized bands near the $E_F$ revealed by the theoretical calculations also support the mechanism of electron-phonon coupling [14,50,51].

## V. CONCLUSIONS

In summary, we have established the high-pressure phase diagram from the initial $B1$ through the intermediate $Pnma$ to the final $B2$ structure for (In, I)-doped PbTe with two superconducting phases with the last two structures. The valence fluctuations and electron-phonon interaction are suggested to account for the superconductivity in the former and latter, respectively.

## ACKNOWLEDGMENTS

The work at HIT was supported by the Shenzhen Science and Technology Program (Grant No. KQTD20200820113045081), the National Postdoctoral Program for Innovative Talents (Grant No. BX2021091), the Basic Research Program of Shenzhen (Grant No. JCYJ20200109112810241), the National Natural Science Foundation of China (Grant No. 51971081), the Cheung Kong Scholar Reward Program Young Scholar Program of China (Grant No. Q2018239), and the Natural Science Foundation for Distinguished Young Scholars of Guangdong Province of China (Grant No. 2020B1515020023). The work at HPSTAR was supported by the National Key R&D Programme of China (Grant No. 2018YFA0305900).

[1] D. Khokhlov, *Lead Chalcogenides: Physics and Applications* (CRC Press, New York, 2002).

[2] A. D. LaLonde, Y. Z. Pei, H. Wang, and G. J. Snyde, Lead telluride alloy thermoelectrics, Mater. Today (Oxford, UK) **14**, 526 (2011).

[3] Q. Zhang, F. Cao, W. S. Liu, K. Lukas, B. Yu, S. Chen, C. Opeil, D. Broido, G. Chen, and Z. F. Ren, Heavy doping and band engineering by potassium to improve the thermoelectric figure of merit in p-type PbTe, PbSe, and $PbTe_{1-y}Se_y$, J. Am. Chem. Soc. **134**, 10031 (2012).

[4] Q. Zhang, Q. C. Song, X. Y. Wang, J. Y. Sun, Q. Zhu, K. Dahal, X. Lin, F. Cao, J. W. Zhou, S. Chen, G. Chen, J. Mao, and Z. F. Ren, Deep defect level engineering: A strategy of optimizing the carrier concentration for high thermoelectric performance, Energy Environ. Sci. **11**, 933 (2018).

[5] J. O. Dimmock, I. Melngailis, and A. J. Strauss, Band Structure and Laser Action in $Pb_xSn_{1-x}Te$, Phys. Rev. Lett. **16**, 1193 (1966).

[6] S. Y. Xu, C. Liu, N. Alidoust, M. Neupane, D. Qian, I. Belopolski, J. D. Denlinger, Y. J. Wang, H. Lin, L. A. Wray, G. Landolt, B. Slomski, J. H. Dil, A. Marcinkova, E. Morosan, Q. Gibson, R. Sankar, F. C. Chou, R. J. Cava, A. Bansil *et al.*, Observation of a topological crystalline insulator phase and topological phase transition in $Pb_{1-x}Sn_xTe$, Nat. Commun. **3**, 1192 (2012).

[7] C. H. Yan, J. W. Liu, Y. Y. Zang, J. F. Wang, Z. Y. Wang, P. Wang, Z. D. Zhang, L. L. Wang, X. C. Ma, S. H. Ji, K. He, L. Fu, W. H. Duan, Q. K. Xue, and X. Chen, Experimental Observation of Dirac-Like Surface States and Topological Phase Transition in $Pb_{1-x}Sn_xTe(111)$ Films, Phys. Rev. Lett. **112**, 186801 (2014).

[8] S. S. Ma, C. Y. Guo, C. C. Xiao, F. Wu, M. Smidman, Y. H. Lu, H. Q. Yuan, and H. Z. Wu, Realization of a new topological crystalline insulator and Lifshitz transition in pbte, Adv. Funct. Mater. **28**, 1803188 (2018).

[9] Y. Matsushita, H. Bluhm, T. H. Geballe, and I. R. Fisher, Evidence for Charge Kondo Effect in Superconducting Tl-Doped PbTe, Phys. Rev. Lett. **94**, 157002 (2005).

[10] Y. Matsushita, P. A. Wianecki, A. T. Sommer, T. H. Geballe, and I. R. Fisher, Type II superconducting parameters of Tl-doped PbTe determined from heat capacity and electronic transport measurements, Phys. Rev. B **74**, 134512 (2006).

[11] M. Matusiak, E. M. Tunnicliffe, J. R. Cooper, Y. Matsushita, and I. R. Fisher, Evidence for a charge Kondo effect in $Pb_{1-x}Tl_xTe$ from measurements of thermoelectric power, Phys. Rev. B **80**, 220403(R) (2009).

[12] T. A. Costi and V. Zlatić, Charge Kondo Anomalies in PbTe Doped with Tl Impurities, Phys. Rev. Lett. **108**, 036402 (2012).

[13] M. Dzero and J. Schmalian, Superconductivity in Charge Kondo Systems, Phys. Rev. Lett. **94**, 157003 (2005).

[14] Y. I. Ravich and S. A. Nemov, Hopping conduction via strongly localized impurity states of indium in PbTe and its solid solutions, Semiconductors **36**, 1 (2002).

[15] A. L. Shelankov and A. F. Ioffe, Mixed-valence behaviour of impurities as a mechanism for superconductivity in IV-VI compounds, Solid State Commun. **62**, 327 (1987).

[16] C. M. Varma, Missing Valence States, Diamagnetic Insulators, and Superconductors, Phys. Rev. Lett. **61**, 2713 (1988).

[17] A. Taraphder and P. Coleman, Heavy-Fermion Behavior in a Negative-$U$ Anderson Model, Phys. Rev. Lett. **66**, 2814 (1991).

[18] K. Nakayama, T. Sato, T. Takahashi, and H. Murakami, Doping Induced Evolution of Fermi Surface in Low Carrier Superconductor Tl-Doped PbTe, Phys. Rev. Lett. **100**, 227004 (2008).

[19] P. Walmsley, C. Liu, A. D. Palczewski, P. Giraldo-Gallo, C. G. Olson, I. R. Fisher, and A. Kaminski, Direct spectroscopic evidence for mixed-valence Tl in the low carrier-density superconductor $Pb_{1-x}Tl_xTe$, Phys. Rev. B **98**, 184506 (2018).

[20] L. C. Chen, P. Q. Chen, W. J. Li, Q. Zhang, V. V. Struzhkin, A. F. Goncharov, Z. F. Ren, and X. J. Chen, Lattice melting and superconductivity in a group IV-VI compound, Phys. Rev. B **103**, 214516 (2021).

[21] N. B. Brandt, D. V. Gitsu, N. S. Popovich, V. I. Sidorov, and S. M. Chudinov, Superconductivity of the compounds PbTe and PbSe under high pressure, JETP Lett. **22**, 104 (1975).

[22] T. Chattopadhyay, A. Werner, H. G. von Schnering, and J. Pannetier, Temperature and Pressure Induced Phase Transition in IV-VI Compounds, Rev. Phys. Appl. **19**, 807 (1984).

[23] G. Rousse, S. Klotz, A. M. Saitta, J. Rodriguez-Carvajal, M. I. McMahon, B. Couzinet, and M. Mezouar, Structure of the intermediate phase of PbTe at high pressure, Phys. Rev. B **71**, 224116 (2005).

[24] Y. C. Li, C. L. Lin, H. Li, X. D. Li, and J. Liu, Phase transitions in PbTe under quasi-hydrostatic pressure up to 50 GPa, High Pressure Res. **33**, 713 (2013).

[25] P. Barone, T. Rauch, D. D. Sante, J. Henk, I. Mertig, and S. Picozzi, Pressure-induced topological phase transitions in rocksalt chalcogenides, Phys. Rev. B **88**, 045207 (2013).

[26] F. J. Kong, Y. H. Liu, B. L. Wang, Y. Z. Wang, and L. L. Wang, Lattice dynamics of PbTe polymorphs from first principles, Comput. Mater. Sci. **56**, 18 (2012).

[27] G. A. Samara and H. G. Drickamer, Effect of pressure on the resistance of PbS and PbTe, J. Chem. Phys. **37**, 1159 (1962).

[28] Y. Fujii, K. Kitamura, A. Onodera, and Y. Yamada, A new high-pressure phase of PbTe above 16 GPa, Solid State Commun. **49**, 135 (1984).

[29] J. J. Ying, V. V. Struzhkin, Z. Y. Cao, A. F. Goncharov, H.-K. Mao, F. Chen, X. H. Chen, A. G. Gavriliuk, and X. J. Chen, Realization of insulating state and superconductivity in the Rashba semiconductor BiTeCl, Phys. Rev. B **93**, 100504(R) (2016).

[30] L. C. Chen, H. Yu, H. J. Pang, B. B. Jiang, L. Su, X. Shi, L. D. Chen, and X. J. Chen, Pressure-induced superconductivity in palladium sulfide, J. Phys.: Condens. Matter **30**, 155703 (2018).

[31] G. Huang, Z. Y. Cao, T. R. Wei, A. F. Goncharov, K. Glazyrin, H. Yu, X. Shi, L. D. Chen, and X. J. Chen, Memory of pressure-induced superconductivity in a phase-change alloy, Phys. Rev. B **103**, 174515 (2021).

[32] X. M. Zhao, Y. H. Zhou, V. V. Struzhkin, H.-K. Mao, A. G. Gavriliuk, X. Y. Qin, and X. J. Chen, Superconductivity in efficient thermoelectric material $Cu_3Sb_{0.98}Al_{0.02}Se_4$, J. Alloys Compd. **890**, 161828 (2021).

[33] C. Prescher and V. B. Prakapenka, Dioptas: A program for reduction of two-dimensional x-ray diffraction data and data exploration, High Pressure Res. **35**, 223 (2015).

[34] V. Petricek, M. Dusek, and L. Palatinus, Crystallographic computing system JANA2006: General features, Z. Kristallogr. - Cryst. Mater. **229**, 345 (2014).

[35] A. G. Gavriliuk, A. A. Mironovich, and V. V. Struzhkin, Miniature diamond anvil cell for broad range of high pressure measurements, Rev. Sci. Instrum. **80**, 043906 (2009).

[36] L. J. van der Pauw, A method of measuring specific resistivity and Hall effect of discs of arbitrary shape, Philips Res. Rep. **13**, 1 (1958).

[37] G. Kresse and J. Furthmüller, Efficient iterative schemes for *ab initio* total-energy calculations using a plane-wave basis set, Phys. Rev. B **54**, 11169 (1996).

[38] J. P. Perdew, K. Burke, and M. Ernzerhof, Generalized Gradient Approximation Made Simple, Phys. Rev. Lett. **77**, 3865 (1996).

[39] F. D. Murnaghan, The compressibility of media under extreme pressure, Proc. Natl. Acad. Sci. USA **30**, 244 (1944).

[40] L. C. Chen, P. Q. Chen, W. J. Li, Q. Zhang, V. V. Struzhkin, A. F. Goncharov, Z. F. Ren, and X. J. Chen, Enhancement of thermoelectric performance across the topological phase transition in dense lead selenide, Nat. Mater. **18**, 1321 (2019).

[41] N. R. Werthamer, E. Helfand, and P. C. Hohenberg, Temperature and purity dependence of the superconducting critical field, $H_{c2}$ III. Electron spin and spin-orbit effects, Phys. Rev. **147**, 295 (1966).

[42] K. Hoang, S. D. Mahanti, and P. Jena, Theoretical study of deep-defect states in bulk PbTe and in thin films, Phys. Rev. B **76**, 115432 (2007).

[43] S. D. Mahanti, K. Hoang, and S. Ahmad, Deep defect states in narrow band-gap semiconductors, Phys. B (Amsterdam, Neth.) **401-402**, 291 (2007).

[44] A. S. Erickson, J.-H. Chu, M. F. Toney, T. H. Geballe, and I. R. Fisher, Enhanced superconducting pairing interaction in indium-doped tin telluride, Phys. Rev. B **79**, 024520 (2009).

[45] M. Kriener, M. Sakano, M. Kamitani, M. S. Bahramy, R. Yukawa, K. Horiba, H. Kumigashira, K. Ishizaka, Y. Tokura, and Y. Taguchi, Evolution of Electronic States and Emergence of Superconductivity in the Polar Semiconductor GeTe by Doping Valence-Skipping Indium, Phys. Rev. Lett. **124**, 047002 (2020).

[46] M. Katsuno, R. Jha, K. Hoshi, R. Sogabe, Y. Goto, and Y. Mizuguchi, High-pressure synthesis and superconducting properties of NaCl-type $In_{1-x}Pb_xTe$ ($x = 0$–$0.8$), Condens. Matter **5**, 14 (2020).

[47] N. Haldolaarachchige, Q. Gibson, W. W. Xie, M. B. Nielsen, S. Kushwaha, and R. J. Cava, Anomalous composition dependence of the superconductivity in In-doped SnTe, Phys. Rev. B **93**, 024520 (2016).

[48] K. Maki, Effect of Pauli paramagnetism on magnetic properties of high-field superconductors, Phys. Rev. **148**, 362 (1966).

[49] X. J. Chen, V. V. Struzhkin, Z. G. Wu, R. E. Cohen, S. Kung, H.-K. Mao, R. J. Hemley, and A. N. Christensen, Electronic stiffness of a superconducting niobium nitride single crystal under pressure, Phys. Rev. B **72**, 094514 (2005).

[50] S. Ahmad, K. Hoang, and S. D. Mahanti, *Ab Initio* Study of Deep Defect States in Narrow Band-Gap Semiconductors: Group III Impurities in PbTe, Phys. Rev. Lett. **96**, 056403 (2006).

[51] K. Hoang and S. D. Mahanti, Electronic structure of Ga-, In-, and Tl-doped PbTe: A supercell study of the impurity bands, Phys. Rev. B **78**, 085111 (2008).